THE JOURNAL OF PHYSICAL CHEMISTRY C
A JOURNAL OF THE AMERICAN CHEMICAL SOCIETY

pubs.acs.org/JPCC

Article

Full-Field and Quantitative Analysis of a Thin Liquid Film at the Nanoscale by Combining Digital Holography and White Light Interferometry

Vincenzo Ferraro, Zhe Wang,* Lisa Miccio, and Pier Luca Maffettone

Cite This: *J. Phys. Chem. C* 2021, 125, 1075−1086

Read Online

ACCESS | Metrics & More | Article Recommendations | Supporting Information

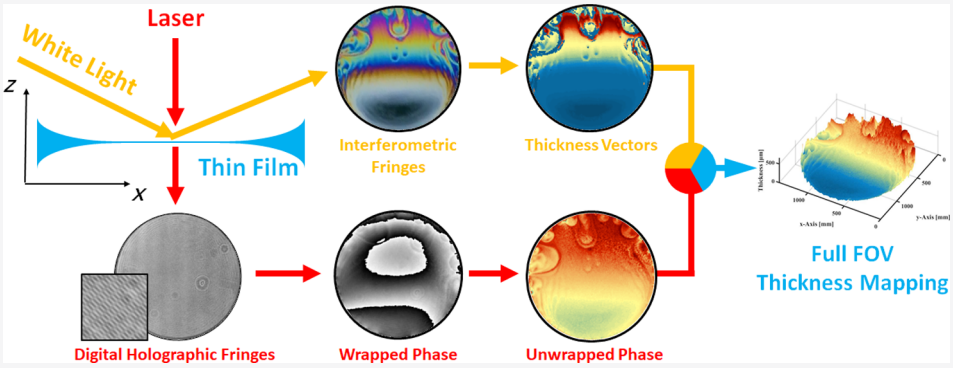

ABSTRACT: Visualizing and measuring thin-film thickness at the nanoscale during dynamic evolution has been an open challenge for long term. Here, a joint-imaging method and the thereof innovative procedure are presented for merging digital holography (DH) and white light colorimetric interferometry (WLCI) measurement data in a single intelligent tool. This approach allows a complete quantitative study of the dynamic evolution of freestanding thin films under high spatial resolution and full-field modality over a large area. By merging interferometric and holographic fringes, it is possible to overcome the lack of DH in thickness measurements of ultrathin layers, providing a reliable reference for full-field quantitative mapping of the whole film with interferometric accuracy. Thanks to the proposed approach, the time-related and concentration-related evolution of surfactant film thickness can be studied. The thickness distribution curves reveal the small changes in the film thickness with time and concentration. The reported tool opens a route for comprehending deeply the physics behind the behavior of freestanding thin liquid films as it provides an in situ, continuous monitoring of film formation and dynamic evolution without limits of thickness range and in full-field mode. This can be of fundamental importance to many fields of applications, such as fluids, polymers, biotechnology, bottom-up fabrication, etc.

1. INTRODUCTION

Thin films are indispensable components of modern manufacturing; from electronic chips to household chemicals, they have accompanied mankind for centuries. Nowadays, even children can simply create a thin film with soap, but we are still looking for effective tools to measure their real-time thickness distribution. Quantitative thickness mapping for thin liquid films has been a widely studied issue over the past decades; visualizing and characterizing thin-film evolution are still long-term open challenges.[1,2] The analysis of thin films and bubbles has traditionally been performed by studying colored fringes resulting from the constructive and destructive interference of a specific wavelength beam; this technique is called thin-film interferometry or even white light interferometry (WLI).[3,4] WLI is a historic and reliable technique with multiple evolutionary branches. Many studies reveal that WLI has the capability to provide accurate local thickness for measurements on smooth films. The reflection appears when the thickness of the film is proportional to a quarter of the recording wavelength so that its axial resolution could reach a quarter of the smallest illumination wavelength. In interferometry, when a transparent region is too thin, the thickness information cannot be probed by the light beam; this area is called black film.[5] Nevertheless, it is possible to determine the thickness of the entire film area by interference fringe recognition and calculating the theoretical value where black films appear during recording under visible light.[6] Note-

Received: October 22, 2020
Revised: December 6, 2020
Published: January 4, 2021

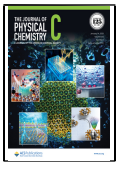

https://dx.doi.org/10.1021/acs.jpcc.0c09555
J. Phys. Chem. C 2021, 125, 1075−1086

worthily, films thinner than 100 nm can be observed with specialized detectors and light sources,[7] and measurement of local film thickness is possible under the assumption that the topographical structure of the film is simple (for example, flat with negligible defects). Nowadays, a major challenge with interferometry lies first in the inability to get accurate absolute thickness measurements when a black film is not presented in the imaging field of view (FOV). The second challenge lies in the difficulty of discerning structural information of the film surface. Typically, studies on thin films make use of very smooth areas with few defects rather than to study structurally complicated thin films.[5] The third challenge is related to the requisite spatial and temporal resolution of thin-film measurement under full FOV, for example, in the case of film instability and bubble rupture.[8] In these experimental cases, to get a complete data set, full FOV imaging is required; however, conventional interferometric technology is difficult to maintain high spatial and temporal resolution for full FOV.[9]

To overcome the above problems, a series of interferometric techniques, including colorimetric interferometry,[6,10] multiwavelength interferometry,[11−16] phase-shift interferometry,[5,17−19] scanning interferometry,[20,21] and so on, have been proposed to address the thin-film challenges. Specifically, the colorimetric interferometry focuses on the challenge in the absolute thickness measurement; under the condition of the known relationship between film thickness and interferometric color scale, the film thickness distribution in a certain range can be extracted.[22] Multiwavelength interferometry mainly meets the needs for temporal resolution and imaging FOV; compared with the colorimetric one, it provides the measurement of complex surfaces with a relatively low spatial resolution. Phase-shift interferometry and scanning interferometry can guarantee high horizontal and vertical resolution at the same time; however, both of them have a abilities on revealing dynamicsweak temporal resolution. The interferometry, digital imaging, and optical microscopy (IDIOM) protocols proposed by Sharma et al. revealed the possibility of achieving dynamic thin-film measurements at high temporal and spatial resolution under certain limits.[23] For small-size freestanding thin films with a maximum thickness lower than a micron scale, IDIOM protocols show powerful capabilities in revealing dynamics of stratification and instability of freestanding films.[24,25] Overall, interferometry-based thin-film measurement tools have been fully studied in the past decade, but the existing approaches cannot meet easily all the needs of thin-film measurement requirements in various scenarios. We still lack measurement methods that have large FOV and high temporal and spatial resolution simultaneously.

In our previous study, as one of the interference imaging technologies, digital holography (DH)[26−29] has been proven to be a reliable experimental method with the requisite spatial (thickness higher than half of the recording wavelength) and temporal resolution for full-field thin liquid film thickness measurements.[30,31] For the continuously growing film, the drainage process of the surface liquid flow can be accurately measured by the transmission DH approach, no matter how complicated the structure of the film is. Even though DH shows the ability to figure out two of the three challenges of interferometry, except for the first challenge mentioned above, it still has three aspects of limitations: (a) holographic recording of the entire life of one thin film is necessary for obtaining accurate thickness distribution, especially the last frame before film rupture when the common black film (CBF)[32] appears in the hologram; (b) areas with local thicknesses less than half of the recording wavelength cannot be accurately recorded without a background reference; (c) due to the lens effect of the thin liquid film itself, it is necessary to build a three-dimensional evolution model of the film to remove phase distortion effectively. Therefore, for some liquid films that break quickly (e.g., low-concentration liquid film) or will not rupture (e.g., protein film), holography is difficult to apply on performing accurate thickness measurements.

As one of the state-of-the-art imaging technologies, DH has shown enough potential to compete for the optimal thin liquid film imaging tool. Here, we show that one possibility for improving thin-film measurements having a suitable tool in all conditions is a fusion approach between WLI and DH. Specifically, both WLI and DH share the same major challenge, i.e., the appearance of CBFs would be a necessary condition for most related thin-film thickness mapping technologies. Fortunately, for a thin liquid film, we notice that the colorimetric calculation of thin-film color fringes is an approach easy to implement and can overcome the black film dilemma in DH. It can provide the thickness of ultrathin areas that are missing in digital holographic measurements when measuring the thickness of the surfactant film.[33,34] Therefore, a wise solution could be to combine DH and colorimetric calculation to increase the thickness measurement range in thin liquid film imaging.

In this paper, we present a fusion method, which combines DH with white light colorimetric interferometry (WLCI), and achieved large FOV (radius > 5 mm), high sensitivity, a wide range of thicknesses (around 100 nm to 10 μm), and high-spatial-resolution thin-film measurement based on a pair of interference images. Thanks to this joint-imaging method, the above-mentioned challenges of holography and interferometry are solved at the same time. Meanwhile, the recording speed of the proposed method depends only on the recording equipment used, which means that high-temporal-resolution thin-film recording could be realized using a high-speed camera. Following our fusion approach strategy, we present a recording geometry that combines an off-axis Mach−Zehnder interferometer and an oblique illumination WLI system. This system uses two cameras and provides digital holograms and WLI interference fringe images simultaneously, thus allowing building the basis for the hybrid numerical reconstruction process that is able to furnish measurements in all of the FOVs without ambiguity. The essential advantage of the proposed hybrid method is that there is no need for CBF thickness self-reference or recording of complete film life cycles, which are indispensable in DH processing. The thickness calculation and calibration could be applied thanks to the fusion of holographic numerical reconstruction process[26,27,30] and the colorimetric fringe pattern process.[35] To prove the capabilities of the proposed approach, we carried out experimental investigations on nonionic surfactant films. A series of time-related and concentration-related tests were performed and revealed the relationship between the film thickness distribution and its dynamic variations. We believe that the technical requirements for dynamic thin-film thickness mapping will expand to more fields and emerging issues, e.g., thin-film dynamics,[36] branched flow of light,[22] controlled pyroelectric tweezers,[37] and so on.

2. METHODS

DH in the off-axis geometry is also based on the holography principle, but different from conventional optical holography,

https://dx.doi.org/10.1021/acs.jpcc.0c09555
J. Phys. Chem. C 2021, 125, 1075−1086

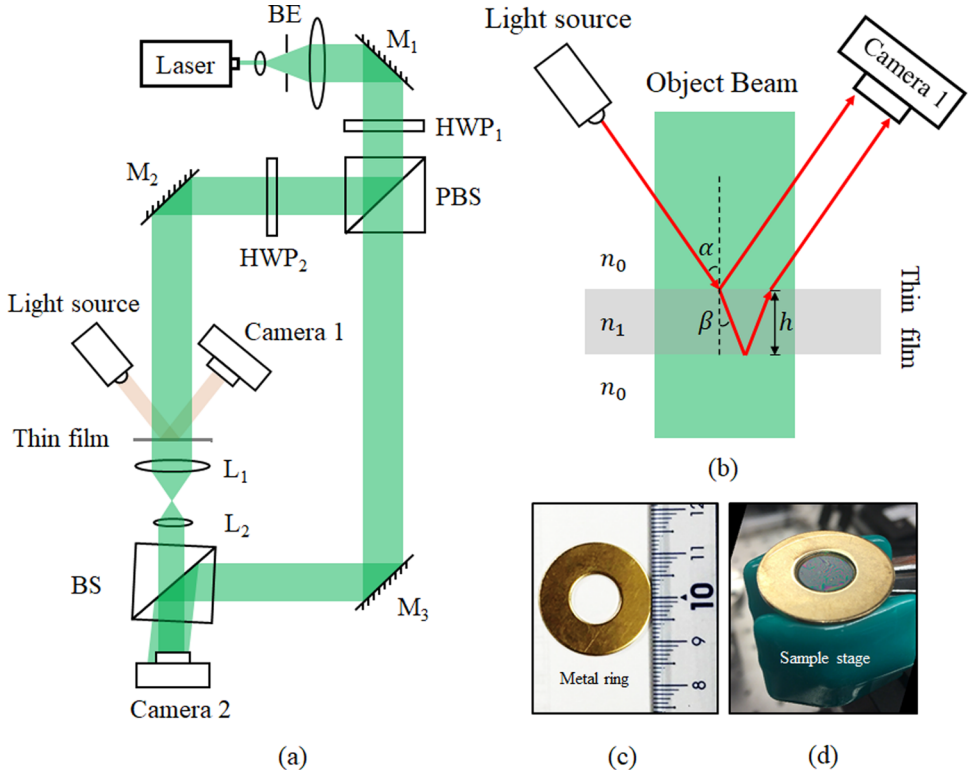

Figure 1. Schematic diagram of the holographic and interferometric hybrid recording setup. (a) Geometry of the recording setup. Laser, a coherent light source of wavelength 532 nm; BE, beam expander; HWP_1/HWP_2, half-wave plates at wavelength 532 nm; PBS, polarizer beam splitter tube for wavelength 400−700 nm; $M_1/M_2/M_3$, mirrors; BS, beam splitter tube for wavelength 400−700 nm; L_1, a convex lens with a focal length of 100 mm; L_2, a convex lens with a focal length of 50 mm; camera 1, a camera for colorimetric interferometric recording; and camera 2, a camera for holographic recording. (b) Principle diagram of thin-film colorimetric interferometry. (c) Metal ring for creating the thin liquid film. (d) Prepared nonionic surfactant film placed on the sample stage.

the recording of digital holograms is performed by a digital camera such as a charge-coupled device (CCD) or a complementary metal−oxide semiconductor (CMOS). The subsequent reconstruction imaging of the holograms is carried out numerically with the holographic reconstruction algorithm in a computer.[28,29] The optical setup for the proposed approach is designed based on an off-axis Mach−Zehnder interferometer with a WLI arrangement to the object arm of the holographic geometry. In this case, DH and WLI recordings can be implemented for the same thin liquid film simultaneously.

As shown in Figure 1a, the optical setup of off-axis transmission DH recording is configured with two coherent beams from a laser source of a wavelength of 532 nm (Thorlabs, CPS532). The laser is divided into two beams by a polarized beam splitter (PBS) prism after being enlarged by a beam expander (BE) structure, where the transmission beam is set as a reference beam and the reflected beam is set as an object beam. The first half-wave plate (HWP_1) is placed in front of the PBS to adjust the splitting ratio of the two beams, and the second half-wave plate (HWP_2) is located behind the PBS to adjust the polarization state of this beam. The thin liquid films are created and held by a metal ring with an inner diameter of 10.52 mm, as shown in Figure 1c. Once the film preparation is completed, the metal ring will hold the film until it ruptures. The sample is placed in the path of the object beam so that its amplitude and phase information can be loaded on the object beam. After passing through the beam splitter prism tube (BS), the object beam and reference beam with a certain angle are combined into optical interference. In addition, a pair of lenses with different focal lengths is placed at a certain distance from the sample, which constituted a 4F system to resize the object beam. Herein, L_1 is a convex lens with a focal length of 100 mm and L_2 is a convex lens with a focal length of 50 mm. A digital single-lens reflex (DSLR) camera without a lens was employed for DH recording (camera 2 in Figure 1), which was a Canon EOS 5D Mark III with 5760 × 3840 pixels of pixel size 6.22 μm. For suppressing the scattering noise from a white light source, the camera's recording parameters were set intentionally as ISO-125, aperture f/0 (no lens), and exposure time 1/1000 s. This setting ensures that the peak intensity of the digital hologram is below 200 units when recorded in the proposed system. For extracting film thickness information using digital holography, thanks to the numerical reconstruction process, the relative phase information of the thin-film thickness can be obtained. The phase is based on the optical path length experienced by the object beam, which is equal to the thickness of the film multiplied by its refractive index (RI). Thus, once we reconstruct the phase φ from the digital hologram, the local thickness h of the film can be calculated by formula

$$h = \frac{\lambda\varphi}{2\pi(n_1 - n_0)} \tag{1}$$

where λ is the wavelength of the recording beam and n_0 and n_1 are the RIs of air and thin liquid film, respectively. Furthermore, to prove that the white light interferometric recording process will not affect the holographic recording and

https://dx.doi.org/10.1021/acs.jpcc.0c09555
J. Phys. Chem. C 2021, 125, 1075−1086

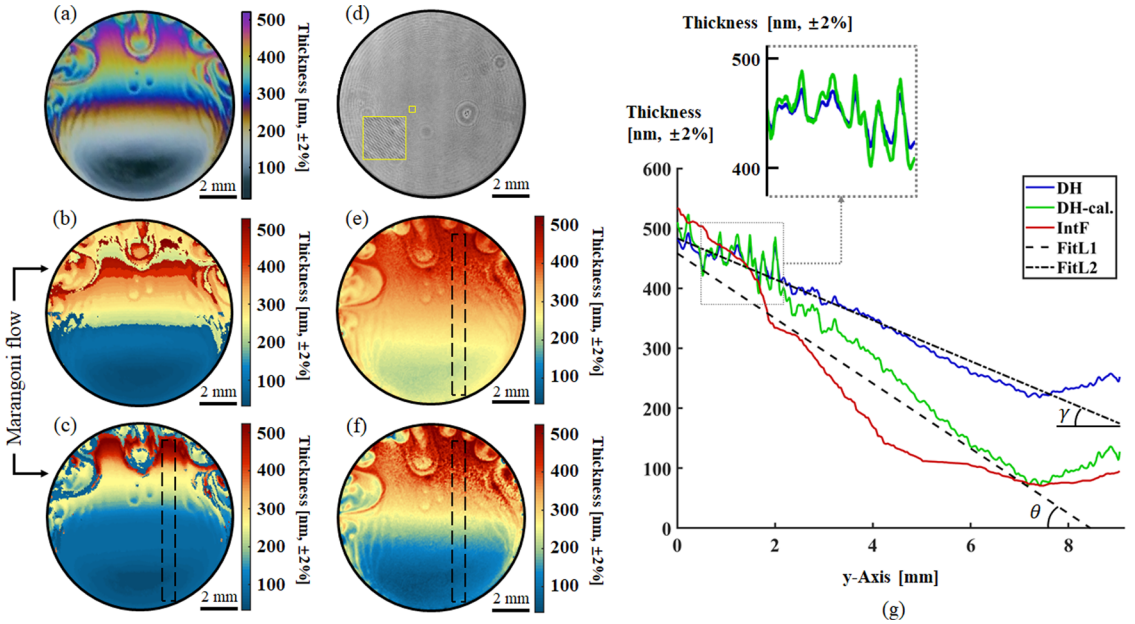

Figure 2. Experimental results of the last frame before rupture recorded by DH and thin-film WLCI. (a) WLI imaging result. (b) WLCI thickness distribution based on the standard Newton color scale of the surfactant film. (c) WLCI thickness distribution based on self-reference colorimetric interferometry. (d) Digital hologram; the zoomed-in area reveals the interference fringes. (e) Holographic thickness distribution before calibration. (f) Holographic thickness distribution calibrated by the WLCI result in (c). (g) Average thickness curves in selected areas; the red curve, named as IntF, is extracted from (c), the blue curve, named as DH, is extracted from (e), and the green curve, named as DH-cal., is extracted from (f).

show the reliability of the proposed system, a transparent poly(methyl methacrylate) (PMMA) phase grating with the known refractive index and structure information was recorded by the DH method; please refer to Supporting Information B.

The optical geometry of thin-film WLI in the hybrid recording setup follows the conventional side-illumination structure.[38] The white light source, which is an incoherent light source, and the camera with an automatic zoom configuration are placed on the top side at a certain angle to constitute the entire structure, as shown in Figure 1b, where α is the angle of incidence, which is 37.3° in our setup; β is the angle in the film, which could be calculated by Snell's law from α and the known refractive index; and h is the local thickness of the film. In this case, the white light beam emitted by the light source is reflected by the upper and lower surfaces of the film and then creates multicolor interference fringes. A CMOS camera was employed as camera 1 for interferometry recording, which was a Sony Exmor RS IMX315 with 4320 × 3240 pixels of pixel size 1.22 μm. Once we illuminate the thin film with white light, the observation color at a specific angle is related to its thickness, and it also upon the angle of view. The visible light part will be converted into color information when a digital camera is used to record the reflected light waves. Thus, based on the hypothesis of known RIs, the thickness of the thin film can be obtained by formula

$$h = \left(m - \frac{1}{2}\right)\frac{\lambda_r}{2n_1 \cos\beta} \tag{2}$$

where λ_r is the wavelength of the reflected beam and m is the order of wavelengths, related to the Newton color scale. For some special films, such as surfactant films, the relationship between the thickness and the recorded color under vertical white light illumination has been obtained through experiments and simulations.[33] Therefore, we can establish a clear one-to-one correspondence between the thickness and the recorded color under certain illumination angle α. Based on this correspondence, for the color fringes of the same surfactant films under a specific illumination angle, we can obtain the thickness information through color comparison; this method is known as WLCI.

In our setup, DH and WLI geometries record the same area of the film after fine adjustments; it is the foundation for the fusion and comparison of the two methods. The irradiation power of the white light source is 8 μW and the laser power is 0.26 mW on the same plane, which is ≈32 times that of white light. Under this condition, the influence of the signal-to-noise ratio (SNR) on hologram recording caused by white light scattering is less than 3%. In addition, a set of shutter sounds of the DSLR camera were used to synchronize the recording time between the two different methods. Even so, a slight difference in the recording time was still unavoidable, which was caused by the unstable shutter speed of the DSLR camera during continuous recording but can be adjusted by framerate matching (IMX315, 30 fps; EOS 5D Mark III, 5 fps).

Based on the hybrid recording system, as shown in Figure 1, a thin-film thickness extraction approach is proposed, which combines thin-film digital holographic thickness reconstruction with colorimetric processing in WLCI. To perform the fusion thin-film thickness calculation approach, DH and WLI are used to obtain the measurement results at the same FOV and recording time. Thus, the complementary characteristics of DH and WLI act as the core of fusion thickness calculations. The lateral resolution will depend on the DH setup, while the axial resolution depends on both DH and interferometry: once the film thickness is below half of the recording wavelength, the axial resolution depends on interferometry, otherwise relies on DH. Compared with two independent methods, the fusion approach can satisfy the following issues: (a) thickness calculation regardless of the presence of the black film; (b) phase calibration in DH no longer uses background

https://dx.doi.org/10.1021/acs.jpcc.0c09555
J. Phys. Chem. C 2021, 125, 1075−1086

subtraction; (c) the lower limit of the measurement range is determined by WLI, while the upper limit is ensured by DH, thus significantly extending the measurement range; and (d) the measurement of complex thin-film structures with high temporal and spatial resolution is achievable. In other words, this hybrid method can meet all of the challenges in the measurement needs of thin films.

Taking 60 mg/L Merpol solution to form a thin liquid film, a pair of digital holograms and color interference fringes was recorded when the thin film was close to rupture and then they were processed by different approaches; the results are shown in Figure 2. The reason to choose this time point is that it has a large black film area, where DH is unable to provide accurate thickness mapping once the thickness is lower than 266 nm.

In Figure 2, the results of DH and WLI were obtained at approximately the same time and then the thickness of the pair of data was calculated by independent digital holographic reconstruction, interference colorimetry, self-reference colorimetry, and the proposed approach. Figure 2a shows the original WLI result and the corresponding color−thickness scale in the ideal state (which does not consider the color differences introduced by the recording camera). A big black film is presented in the lower part of FOV. As seen from the colorimetric gradation, the thickness of the black film area in WLCI is less than 100 nm; Figure 2b,c shows the full-field thickness distribution calculated by colorimetry. In these cases, different colorimetric scales are used: (a) For Figure 2b, the thickness is calculated from the standard Newton color scale of the surfactant film. Herein, the mismatch between the standard color scale and the recorded colors causes a discontinuous distribution of the thickness; this is related to the insufficient color resolution of the CMOS chip. (b) For Figure 2c, the color scale is extracted from a continuously changing color band in Figure 2a and then compared and assigned to the existing color levels to optimize results; hence, the thickness distribution shown in Figure 2c smoothly changes. We named this approach as thin-film self-reference colorimetric interferometry (in Supporting Information A). However, the accuracy of thickness calculation for complex surfaces from the self-reference colorimetry method is poorer than that of the conventional one because complex surfaces usually require more accurate color resolution. This is the well-known drawback of the self-reference method. As seen from the region affected by Marangoni flow in the upper left corner of Figure 2c, the thickness distribution of the corresponding area could not be calculated due to the lack of color scales in self-reference color colorimetry.

Figure 2d,e shows the digital hologram of the recording area and the corresponding thickness distribution, respectively. The thickness map is reconstructed following the approach from a previous study.[30] Comparing the results in Figure 2e,c under the same color scale, there is a vast difference in the local thickness of the black film. As mentioned before, independent transmission holography cannot accurately reveal the local thickness, where less than half of the recording wavelength occurs (herein, around 266 nm) without the aid of reference points; it is providing an incorrect quantitative profile in Figure 2e. However, self-reference colorimetric interferometry provides more reliable thickness distribution results, as shown in Figure 2c. Thus, the WLCI results can be used to adjust the local thickness in holographic results.

To calibrate the thickness by holographic measurements, the effective thickness areas need to be extracted from WLCI results, thus fitting the thickness distribution of each area to get the trends. These trends will calibrate the holographic thickness distribution and can also be converted to an equivalent phase according to eq 1, so allowing for phase distortion calibration. Generally, off-axis DH geometry involves three types of phase distortions: (a) first-order phase distortion generated by the off-axis phase angle, (b) second-order phase distortion introduced by the optical system, and (c) second-order phase distortion related to the lens effect of the thin film. These three distortions are treated as one higher-order phase distortion to be removed because they are difficult to process separately. For the measurement in Figure 2, the y-direction thickness calibration is taken as an example to show the calibration processing. The area within the dotted frame from Figure 2c is extracted and the thickness value is averaged along the x-direction. As a red line shown in Figure 2g. The range of the y-direction average thickness of the dotted frame area in Figure 2c is from 100 to 550 nm; it is a reliable thickness distribution measured by WLCI. The black film in DH will appear in the areas where thicknesses are less than 277 nm. For these areas, WLCL can reveal the thickness vector when they are smooth enough. Therefore, the holographic thickness vector taken from the same film area shows poor measurement results, as the blue line in Figure 2g. The y-directional holographic thickness vector shows a false trend; thanks to the WLI results in Figure 2a, we know that this lift is unreasonable, and it could be an error caused by holographic numerical phase dedistortion processing.

The core of thickness calibration is the conversion of two thickness vectors. First, sparse sampling is performed on the two thickness vectors; then, the thickness distribution of the corresponding coordinates is linearly fitted in related curves. As a result, the slope $\tan\gamma$ of the holographic thickness fitting curve and the slope $\tan\theta$ of the interferometric thickness fitting curve are obtained. The thickness calibration can be performed according to the following equation

$$h'_{\mathrm{DH}} = \frac{\tan\theta}{\tan\gamma}(h_{\mathrm{DH}} - h_{\mathrm{DH\_min}}) + h_{\mathrm{WLCI\_min}} \tag{3}$$

where h'_{DH} represents the holographic thickness after calibration from h_{DH}, $h_{\mathrm{DH\_min}}$ represents the minimum thickness of the selected area in the holographic results, and $h_{\mathrm{WLCI\_min}}$ represents the minimum thickness of the selected area in interferometry results. Furthermore, due to the linear relationship between the phase and thickness in the holographic thickness calculation, the above thickness calibration process could be converted into a phase distortion calibration process

$$\varphi' = \frac{\tan\theta}{\tan\gamma'}[\varphi - \varphi_{\mathrm{min}}] + \frac{2\pi(n_1 - n_0)h_{\mathrm{WLCI\_min}}}{\lambda} \tag{4}$$

where φ' represents the holographic unwrap phase after calibration from φ, φ_{min} represents the minimum phase value of the selected area, and $\tan\gamma'$ represents the phase slope after fitting and it is equal to $\tan\gamma$. Based on the above process, the holographic thickness vector after calibration is shown as a green line in Figure 2g. Herein, the holographic thickness vector in zone 400−500 nm after calibration shows a rugged curve, and these fluctuations also appear in the conventional holographic measurement result in a blue curve. The blue curve and the green curve maintain a high degree of consistency, as shown in the zoomed-in area in Figure 2g.

https://dx.doi.org/10.1021/acs.jpcc.0c09555
J. Phys. Chem. C 2021, 125, 1075−1086

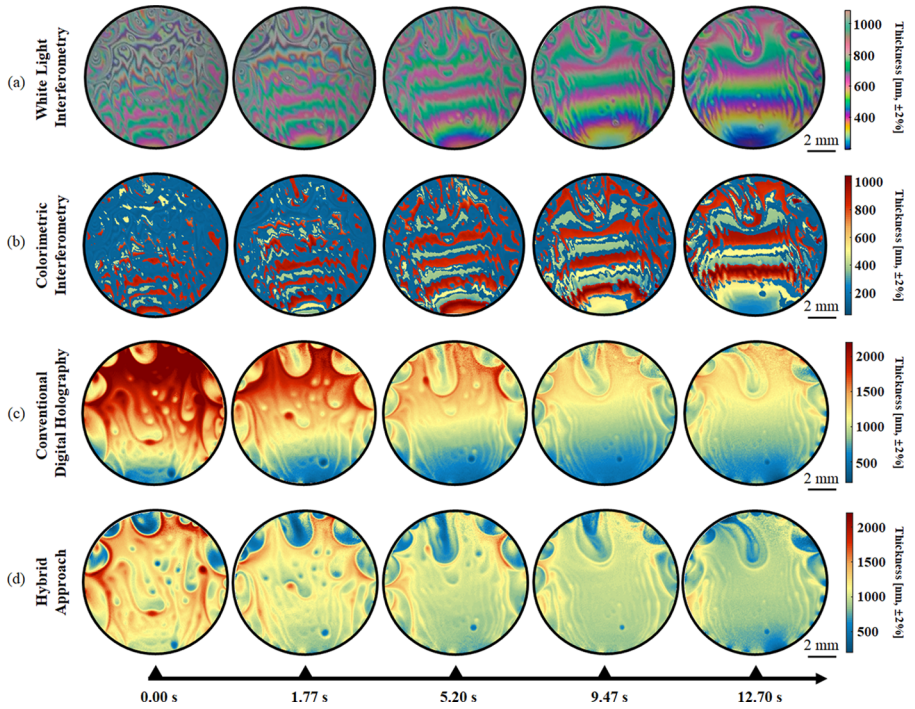

Figure 3. Time-related thickness mapping. Continuously record changes in film thickness using a hybrid method and the recording time points are 0.00, 1.74, 5.20, 9.47, and 12.70 s after film formation. (a) WL results within 12.70 s before the film ruptures. (b) WLCI thickness mapping calculated from (a) in the same time points. (c) Thickness mapping by conventional DH. (d) Thickness mapping by the hybrid DH and WLCI approach.

These ups and downs of the curves are caused by insufficient sampling; this is due to the high-frequency component of the object that is higher than the space-frequency resolution of the sampling CMOS, which can be solved by using a camera with a smaller pixel size (< 4.6 μm) and bigger sensor size to record the holograms.

The thickness calibration for the entire FOV can be achieved by repeated applications of the above procedure, as shown in Figure 2f. By applying the same color−thickness scale, the overall thickness distributions in Figure 2c,f are found to be very close to each other. To verify the effectiveness of different methods, calculating the total volume of the full film area is a good solution for the results in Figure 2. After considering the difference in pixel size (in imaging plane) between different methods, the volumes are calculated: WLCI (standard color scale), 0.021 mm^3; WLCI (self-reference color scale), 0.020 mm^3; DH (conventional), 0.028 mm^3; DH (after calibration), 0.022 mm^3. It is clear that in addition to the conventional holographic method, the thicknesses by the other three methods have maintained a good consistency. This is fully supported evidence that the result after calibration is valid and credible.

Herein, the method not only has the ability to reveal the thickness below half of the recording wavelength, but it can also return the complex surface structure of the calibrated holographic thickness. As it can be seen from Figure 2f, the Marangoni flow structure at the edge of the film can be clearly identified, and the CBF area in DH is also revealed accurately. The application of the proposed procedure and the corresponding results can be implemented also in cases where there are multiple CBFs in the FOV or to cases where the thickness distribution is incomplete under WLCI. This is the case, for example, when the local thickness of some areas exceeds the limit of the colorimetric scale in WLCI, e.g., the edge of Marangoni flow in Figure 2c. The entire FOV needs to be divided into several parts according to the effective colorimetric thickness distribution then executing related approach separately, the discrete thickness points provided by the standard colorimetric method is used as a reference point to calibrate the thickness mapping of the holography, so a few available small thickness areas can complete the phase calibration of the holography. In this case, the overall thickness calibration can be carried out by general surface fitting for all the effective areas.

Regarding the experimental materials we used, nonionic surfactants are chosen in our experiments. Surfactants are usually divided into two categories, ionic and nonionic, based on whether they dissociate in an aqueous solution. The ionic surfactants place themselves at the interface in the case of freestanding films. This molecular-scale arrangement generates two charged layers at the interfaces that can repel each other. If a balance between repulsive and attractive forces is reached, then the film is stable and almost flat.[39,40] In contrast, thin liquid films made with nonionic surfactants are more unstable and, in the case of drainage, they are thinner because of the weak repulsive forces. This means that these films will have a more complex and sensitive structure. We used water as a solvent and Merpol as a surfactant to prepare thin liquid films, which have low foaming and low surface tension. For this type of thin surfactant film, the difference in RIs depending on the concentration is tiny, so we set a uniform value of 1.34 for the RI of the Merpol solution used for making the thin liquid film. Herein, Merpol is an alcohol phosphate and it is defined as a nonionic surfactant; it can be used as a detergent and lubricant agent for many materials and in metal processes; meanwhile, it receives growing importance in printing inks and coatings. The

https://dx.doi.org/10.1021/acs.jpcc.0c09555
J. Phys. Chem. C 2021, 125, 1075−1086

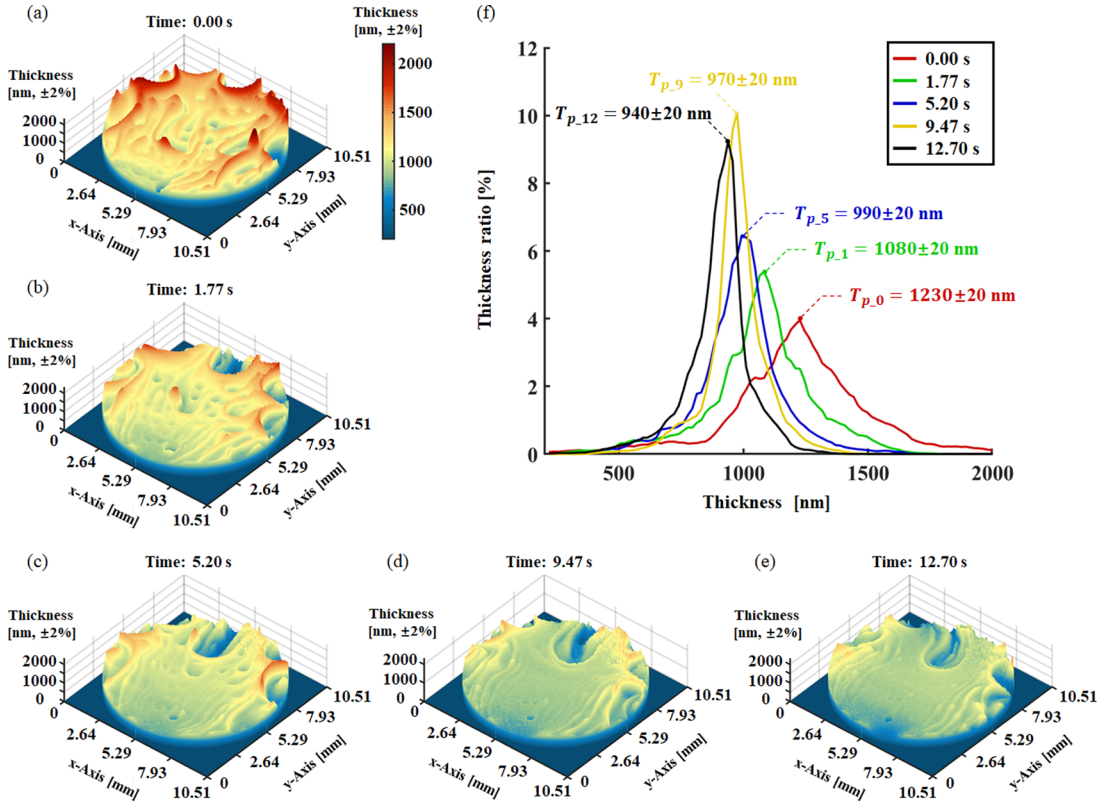

Figure 4. Fusion DH and WLCI approach reveals the dynamic process of the thin liquid film over time. (a−e) 3D thickness mapping of five selected time points. (f) Time-related thickness distribution curves; different colored curves represent different time points after the recording started.

main reason for choosing Merpol as a surfactant is that the thin film will have a complex and changing structure, which is very suitable for judging the ability of the imaging approach. In our case, the major force that causes drainage inside the film is the gravitational one due to tilting of the film. Capillary forces and surface interactions shape the local structure of the surface, producing fingerings and spiral-like geometries, as displayed in Figures 2, 3, and 5.

3. RESULTS AND DISCUSSION

Herein, we present two sets of data recording, reconstructions, and analyses by the fusion DH and WLCI approach, showing the advantages of the fusion method in thin liquid film thickness mapping. The proposed approach has high measurement sensitivity for film thickness changes, allowing a quantitative analysis of film thickness mapping in full FOV. Comparing with thin-film holographic thickness mapping, the proposed method has a larger axial measurement range, which means that the thickness distribution of the film, even though it will rupture soon or never rupture, can be accurately mapped. In addition, comparing with interferometric thickness mapping, the proposed method can provide more detailed information on the thickness distribution of the film, e.g., thickness of the Marangoni flow area. Meanwhile, for some factors that only cause a slight change in the thickness distribution, such as film concentration, the fusion method has the possibility of accurately revealing the tiny changes in thickness distribution.

In time-related thin-film evolution, thickness dynamic mapping of a thin liquid film was studied and analyzed by a hybrid approach. As said, a 60 mg/L Merpol solution was used to form the film. In Figure 3, a set of continuously recorded experimental results is shown. Recording started when the thin liquid film was placed on the sample stage and ended after the film ruptured. Gravity was the only applied external force that caused film drainage and thinning. After 12.80 s, the film ruptured. During the entire recording cycle, five time points were selected (0.00, 1.77, 5.20, 9.47, and 12.70 s), and the thickness distribution from four different thickness mapping methods, WLI, WLCI, conventional DH, and hybrid approach, is shown in Figure 3a−d, respectively. In the areas where the average thickness of the film was larger than ∼1 μm or where the surface of the film was complex, the WLI interference measurement would hardly provide an accurate and complete thickness distribution. There, however, the DH still worked well. This set of images highlights the main differences: the thinner the film (less than half of the recording wavelength), the more reliable the thickness mapping given by interferometry; the thicker the film (thicker than the recording wavelength), the more comprehensive and detailed the thickness mapping given by DH.

The frames in Figure 3a are WLI results after size correction; they reproduce the color−thickness scale based on the Newton color scale with a recording angle of 37.5°. For the surfactant films we used, the recognizable maximum thickness measured with WLI was always below ∼1.5 μm. However, the CMOS chip used was hard to record the right three-channel intensity values when the color fringes showed multiple green−pink interleaved bands so that the consequence was a thickness cutoff of around 1 μm. As shown in Figure 3a, it is difficult to identify the local thickness at 0.00 and 1.77 s; however, for the 5.20, 9.47, and 12.70 s frames, the local thickness is easy to

https://dx.doi.org/10.1021/acs.jpcc.0c09555
J. Phys. Chem. C 2021, 125, 1075−1086

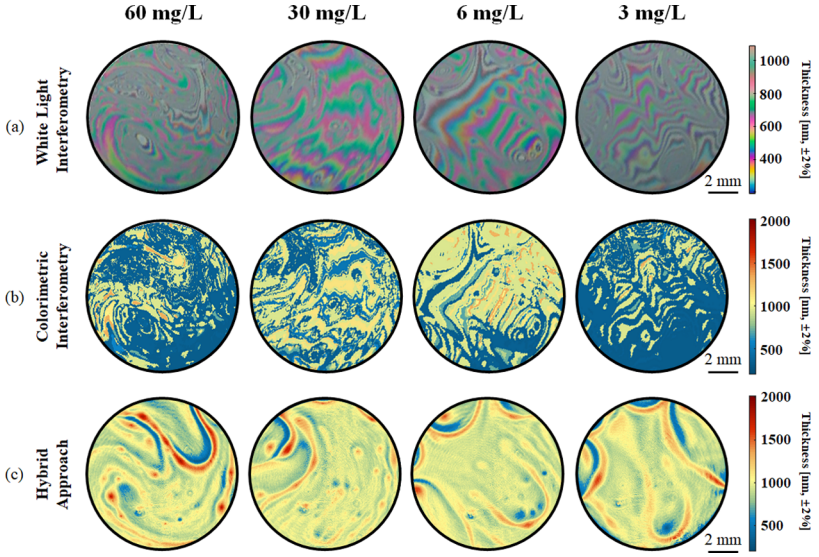

Figure 5. Concentration-related thickness mapping. For thin films of different concentrations of the solute (60, 30, 6, and 3 mg/L), thickness mapping is measured at a certain time point, at 7 ± 1 s before the film rupture. (a) WLI results at four different concentrations. (b) WLCI thickness mapping calculated from (a). (c) Thickness mapping by the hybrid DH and WLCI approach.

detect in the central region of the film because of its smooth distribution. It should be noticed that the periodic green−pink bands represent a smooth area with almost the same thickness, and it relates to the interference fringes of interferometric recording.[41]

Herein, we were not able to find in any frame an ideal thickness vector for a self-reference color scale, so that the film thickness colorimetric calculation processing was based on the standard Newton color scale. Unfortunately, due to the insufficient color resolution of CMOS chips we adopted, the thickness distribution in snapshots of all five time points are not continuous, as shown in Figure 3b. Herein, in the first frame of Figure 3b, we were not able to determine the local thickness of most areas in the FOV. This could be due either to regions with local thicknesses larger than 1 μm or to the presence of regions with complex surfaces. Interestingly, what we can observe from the results in Figure 3b is that the areas where can be used to calculate the effective thickness are growing due to the general thickness decreases with the drainage process. In the thickness mapping at 12.70 s, we find out the thickness information in over 82% FOV, and this value is only 13% at 0.00 s.

The frames in Figure 3c are calculated by the conventional DH method of previous works.[30,31] For conventional holographic thickness processing, the black film has to be found in the last frame of the recorded hologram. In this case, we could only assume that the thickness of the edge of the black film was half of the recording wavelength. Comparing with the results of interferometry in Figure 3b,d, the result calculated by DH shows a distortion. Especially at 12.70 s, the local thickness of the upper part of the film is close to 1.5 μm; however, from the results of WLI and WLCI, the thickness should be around 1 μm. Nonetheless, conventional DH provides full-field thickness mapping for each frame, either when the film is too thick or when the film structure is complex so that once we compare the interferometric images with those obtained by DH for a flat film, we will find a good agreement between the film structures. However, when the film structure is more complex, DH becomes the best choice as a tool for the local film structure evaluation.

The frames in Figure 3d are thickness mapping from the present hybrid approach. The local thickness vectors, from WLCI results, were used to calculate the corresponding thickness from DH. The thickness vectors can also give distortion calibration in the related areas. So, through Figure 3d, we can get the continuous and correct thickness distribution in the five selected times. The general thickness continues to decrease, and the film structure becomes smoother. The thickness mapping at 5.20 s is the dividing point between interferometric and holographic methods in selected frames. There are more than 50% unresolved FOV in WLCI results before this time point, but DH still has the ability to provide the full-field thickness distribution. In addition, the thickness mapping of flows is restored by the hybrid approach: a liquid flow approaching the film center is observed, with a consequent thickening. Thanks to the fusion processing of the WLI and DH results in Figure 3a,c, not only thickness mapping but also the film structure are revealed. In Video S1, the time-related thickness evolution of the results of Figure 3a,d is shown.

To better analyze the time-related results, three-dimensional (3D) thickness mapping of five selected time points is revealed in Figure 4a−e. The concave bubbles, liquid flows, and drainage phenomena on the thin film can be clearly observed. In addition, the change trend of the overall thickness of the film can be judged by the color related to the thickness. From each curve of Figure 4e, the principal thickness T_p of the corresponding FOV can be extracted, which is the thickness with the highest distribution rate. As time goes by, the principal thickness of the film continues to decrease from T_{p_0} = 1230 ± 20 nm to T_{p_12} = 940 ± 20 nm. We can estimate the complexity of the surface structure of the film for each frame. The smaller the standard deviation of the curves, the smoother the surface structure of the film. Interestingly, for the last frame before rupture, while the principal thickness of the film reaches the minimum, the film thickness distribution curve becomes lower; it means the complexity of the film structure tends to be smoother when compared with the snapshot in 9.47 s. We observed similar phenomena in related works.[30] In Video S2, the time-related thickness evolution in 3D is shown.

https://dx.doi.org/10.1021/acs.jpcc.0c09555
J. Phys. Chem. C 2021, 125, 1075−1086

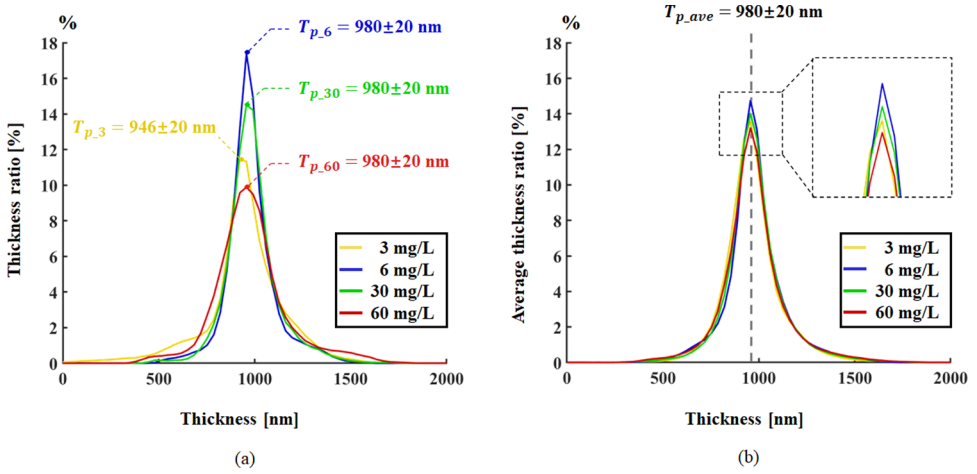

Figure 6. Concentration-related thickness distribution curves; different colored curves represent different concentrations. (a) Single-frame thickness distribution curves, using the corresponding frame in Figure 5c. (b) Thickness distribution curves from the average of multigroup experiments. We perform three sets of experiments for each concentration, and each set of experiments takes three consecutive frames at the same time zone for average calculation. We define the highest point of the curves as the principal thickness.

The above experimental results show that the hybrid method has a higher thickness measurement range during full-field thin-film imaging, and the thickness mapping of complex structures on the films is revealed in time-related experiments like the Marangoni flows.

In concentration-related thin-film evolution, the hybrid approach successfully revealed the change in film structure caused by a concentration difference. Figure 5 shows the results at different Merpol concentrations from 60 mg/L to 3 mg/L, which are 60, 30, 6, and 3 mg/L. We repeated the experiments three times for each concentration to draw the average thickness distribution curves. The frames were selected around 7 ± 1 s before rupture in repeated experiments. Herein, the relationship between the thickness and film structure changes and different concentrations is revealed.

The frames in Figure 5a show thickness mapping at different concentrations from WLI measurements. It is apparent that at different concentrations dissimilar surface structures appear at similar times. By decreasing the solute content from 60 to 6 mg/L, the surface structure of the film turns smoother but film thickness fluctuations increase at 3 mg/L concentration. The same trend was observed in Figure 5b,c. The frames in Figure 5a show thickness mapping from WLCI and those in Figure 5c show thickness mapping from the hybrid approach, and they share the same color−thickness scale. Figure 5b reveals the change in film structure with concentration 60 mg/L; less than 50% area can be used to extract the thickness, and the effective calculated area is higher than 80% of FOV at concentration 6 mg/L. Under this experimental setup, the main forces that induce changes in the film are disjoining pressure, viscosity, surface tension, and gravity. Gravity force drains the liquid from the higher part of the film to the lower and generates the usual thickness gradient as shown in Figure 3c. Once the film becomes thinner, repulsive forces come into play.[39,42] They arise from the negative charges adsorbed at the air−water interface.[43] As a consequence, the thinner part is flatter and more stable. The complexity of the thicker parts stems from the combination of the Marangoni flows,[44] gravity,[45,46] drainage from the plateau border,[39,47−51] and disjoining pressure.[39,42] The result for the 3 mg/L concentration is very peculiar and is due to the very low surfactant content of the film at this concentration.

Herein, it is possible to observe the thickness distributions for four different concentrations in Figure 6, where Figure 6a is calculated from the single snapshot and Figure 6b is calculated from the average of three frames. The frames are taken from repeated experiments for three groups but with the same recording time before rupture. In every analyzed frame, it could be observed that as the surfactant concentration decreases, the thickness uniformity increases except for the last case (3 mg/L). Such observation is also confirmed by the distribution in Figure 6b, which reveals the multigroup average result. For the cases at 60, 30, and 6 mg/L, film inhomogeneity is related to the amount and sharpness of "valleys" and "peaks", as shown in Figure 5c, and this kind of conformation is caused, probably, by a more pronounced marginal regeneration phenomenon as the tensioactive concentration increases.[41,43,49] In the case of 3 mg/L in Figure 5c, there are more valleys (blue regions) and yellow distribution; in Figure 6a, there is a higher amount of thinner regions. The thinner regions correspond to the regions where the attractive forces (Van der Waals interactions) are more pronounced between the two free surfaces. When the surfactant concentration is too low, the surface geometries can be easily disturbed. Herein, no matter how the concentration changes, the hybrid method provides a stable mapping of thin liquid film structure; this creates the possibility for further data analysis, as shown in Figure 6.

The average thickness curve shows high uniformity, where the principal thickness of different concentration films is concentrated at T_{p_ave} = 980 ± 20 nm. Meanwhile, the principal thickness percentage gradually increases as the concentration decreases from 60 to 6 mg/L in the frames we analyzed. This reveals that as the concentration decreases, the film tends to become smoother. Although 3 mg/L exhibits a different type of behavior, this is valuable information because it explains the possibility of further research on the properties of thin films using related methods. By comparing Figure 6a,b, a notable phenomenon is the difference between single-frame results and multiframe average results. Herein, this difference implies the necessity of a large number of experiments in the microfluidic study of thin liquid films; meanwhile, it also

https://dx.doi.org/10.1021/acs.jpcc.0c09555
J. Phys. Chem. C 2021, 125, 1075−1086

reveals that the measurement result error caused by the instability of nonionic thin films can be eliminated by multitime measurements.

Herein, one optical tool successfully reveals the full-field thickness mapping related to the liquid film concentration, and the thickness distribution characteristics of the film can be clearly identified. In particular, the curves in Figure 6 strongly evidence that the proposed method is an effective tool that can meet the needs of liquid film measurement experiments with high spatial and temporal resolution. It is important to note that the accuracy of thickness calibration mostly depends on color recognition of the camera. So, care should be adopted for choosing the camera. It is important to synchronize the acquisitions between the cameras, and a further step of improvement regards the implementation to guarantee dual-camera recording. In this case, interpolation could be a worth-trying solution. In the next step of this study, we will keep searching for the joint points of DH and other thin-film mapping approaches and further optimize the related methods. Also, for some solid films that can simulate the color scales,[51] we suppose that this method will also be applicable but still needs further experiments.

4. CONCLUSIONS

In this paper, we present a fusion approach to map the thin-film thickness; it combines DH and WLCI, both implemented on a thin liquid film simultaneously. We introduced the recording system, the joint reconstruction processing of this method, and a series of thin liquid film measurement experiments based on this approach were performed. As a result, this hybrid method demonstrates powerful measurement capabilities on dynamic liquid film measurements. It reveals the time evolution of the film and how the nonionic surfactant film structure is affected by the concentration.

Comparing with existing interferometric methods, the presented approach could achieve full-field, large-FOV dynamic measurements at the nanoscale, and it could accurately restore the thickness information of the film without relying on the CBF. As far as we know, this is the first time that the challenges of holographic and interferometric thin-film measurements are solved under real-time thickness mapping. Herein, based on the information obtained by WLCI, the calibration frame was made for the information obtained by DH; in contrast, DH provided complete thickness division information, which was not available in conventional interferometric methods. In comparison with our previous study on thin-film holographic measurements, the presented approach could tackle the shortcomings in thin-film digital holographic recording and reconstruction: (a) thickness information can be revealed without relying on full life cycle recording; (b) the thin-film area, where the thickness is less than half of the wavelength, can be measured; (c) film thickness calibration could be achieved without using background subtraction; meanwhile, the background hologram is not a necessary item in the holographic recording process.

In particular, we report that the general thickness of the film will become thinner as the duration of the film evolution increases, but its structural dynamics is indeed quite complex. Meanwhile, the concentration is another factor that affects the film thickness distribution; as the concentration decreases, the film thickness distribution, recorded at the same recording time point, will be smoother generally. We referred to the highest points of the curves in Figures 4 and 6 as principal thicknesses. All of the above experiments were based on the proposed hybrid method and prove its reliability and accuracy.

In the experiment on the time−thickness relationship, we showed the film thinning process. Meanwhile, we analyzed the thickness distribution of the film's full FOV, and we showed the thickness distribution curves for different time points. The results revealed two phenomena: (a) the principal thickness of the film gradually decreased with time; (b) in all cases shown here, the thickness distribution of the film becomes more homogeneous over time, but it gets more complicated just before rupture.

By comparing the thickness distribution of films with different concentrations at specific time points, the corresponding curves were drawn. In the results, the single-group experiment curve and the three-group experiment homogenization curve showed different shapes but the same trends. The principal thickness of the film remained at the same level for the relevant time, but the thickness distribution changed in a nonlinear way. Herein, the presented hybrid approach successfully revealed the tiny differences in morphology caused by the surfactant concentration and provided a reliable database for the development of related research. Furthermore, it can allow the evaluation of the surfactant concentration by measuring the film thickness distribution and so on.

In addition, these parallel experiments could also provide a reference when we have to make a choice between DH and interferometry. We had digital holographic and interferometric data side-by-side at different time points and surfactant concentrations. For thin films that are relatively flat and defect-free, both techniques can be used, and a comparison between the two shows good agreement. It could be even suggested that when films are very thin, interferometry is the better choice because it is possible to observe thicknesses a quarter of the wavelength of the recording beam. However, for more complicated surface structures and when films are thicker, interference patterns are difficult to make sense of or are absent. In these situations, DH is the better choice.

To sum up, the presented approach will provide an independent thin liquid film measurement process and does not require any additional recording conditions, e.g., full life cycle recording or limited measurement range. The relevant thickness extraction process combines DH and WLCI, and the real-time thickness mapping of a thin liquid film can be achieved. Thanks to the time−thickness and concentration−thickness experiments on nonionic surfactant films, the proposed method's full-field sensitive measurement capability is verified. Meanwhile, based on these experimental data, the thickness ratio variation curves are drawn, and these curves reveal the variation of the films in statistics.

We believe that this method will open the way to wide uses of interferometric characterization in the fields of materials science, applied chemistry, and biomaterials at the nano- and microscale, making possible full and quantitative characterization of the dynamic evolution of liquid films and thus helping investigation and understanding of related phenomena.

■ ASSOCIATED CONTENT

Supporting Information

The Supporting Information is available free of charge at https://pubs.acs.org/doi/10.1021/acs.jpcc.0c09555.

Generation of self-reference color scale (Figure S1), full field of view thickness mapping based on the self-

https://dx.doi.org/10.1021/acs.jpcc.0c09555
J. Phys. Chem. C 2021, 125, 1075−1086

reference color scale (Figure S2), and digital holographic thickness mapping for PMMA phase grating (Figure S3) (PDF)

Time-related thickness evolution of the results (Video S1) (AVI)

Time-related thickness evolution in 3D (Video S2) (AVI)

AUTHOR INFORMATION

Corresponding Author

Zhe Wang − *Department of Chemical Engineering, Materials and Industrial Production, University of Naples Federico II, 80125 Napoli, Italy; Institute of Applied Sciences and Intelligent Systems "E. Caianiello", Italian National Research Council (ISASI-CNR), 80078 Pozzuoli (Napoli), Italy;* orcid.org/0000-0002-0593-0413; Email: z.wang@isasi.cnr.it

Authors

Vincenzo Ferraro − *Department of Chemical Engineering, Materials and Industrial Production, University of Naples Federico II, 80125 Napoli, Italy*

Lisa Miccio − *Institute of Applied Sciences and Intelligent Systems "E. Caianiello", Italian National Research Council (ISASI-CNR), 80078 Pozzuoli (Napoli), Italy*

Pier Luca Maffettone − *Department of Chemical Engineering, Materials and Industrial Production, University of Naples Federico II, 80125 Napoli, Italy*

Complete contact information is available at: https://pubs.acs.org/10.1021/acs.jpcc.0c09555

Author Contributions

The manuscript was written through the contribution of all authors. All authors have given approval to the final version of the manuscript. V.F. and Z.W. contributed equally to this work.

Funding

The research has been partly funded by Project PRIN 2017—Morphological Biomarkers for Early Diagnosis in Oncology (MORFEO) Prto. 2017N7R2CJ, and MIUR PON Project 2014−2020 PROSCAN.

Notes

The authors declare no competing financial interest.

ACKNOWLEDGMENTS

This work was supported by the University of Naples Federico II and the Institute of Applied Sciences and Intelligent Systems "E. Caianiello", Italian National Research Council (ISASI-CNR).

REFERENCES

(1) Nikolov, A. D.; Kralchevsky, P. A.; Ivanov, I. B.; Wasan, D. T. Ordered micelle structuring in thin-films formed from anionic surfactant solutions: II. Model development. *J. Colloid Interface Sci.* **1989**, *133*, 13−22.

(2) Mysels, K. J. Soap Films and Some Problems in Surface and Colloid Chemistry. *J. Phys. Chem. A.* **1964**, *68*, 3441−3448.

(3) Israelachvili, J. N. Thin-film studies using multiple-beam interferometry. *J. Colloid Interface Sci.* **1973**, *44*, 259−272.

(4) Lin, C.; Sullivan, R. F. An application of white light interferometry in thin-film measurements. *IBM J. Res. Dev.* **1972**, *16*, 269−276.

(5) Greco, V.; Lemmi, C.; Ledesma, S.; Molesini, G.; Puccioni, G. P.; Quercioli, F. Measuring soap black films by phase shifting interferometry. *Meas. Sci. Technol.* **1994**, *5*, 900.

(6) Afanasyev, Y. D.; Andrews, G. T.; Deacon, C. G. Measuring soap bubble thickness with color matching. *Am. J. Phys.* **2011**, *79*, 1079−1082.

(7) Glovnea, R. P.; Forrest, A. K.; Olver, A. V.; Spikes, H. A. Measurement of sub-nanometer lubricant films using ultra-thin-film interferometry. *Tribol. Lett.* **2003**, *15*, 217−230.

(8) Tammaro, D.; Pasquino, R.; Villone, M. M.; D'Avino, G.; Ferraro, V.; Di Maio, E.; Langella, A.; Grizzuti, N.; Maffettone, P. L. Elasticity in bubble rupture. *Langmuir* **2018**, *34*, 5646−5654.

(9) Frostad, J. M.; Tammaro, D.; Santollani, L.; de Araujo, S. B.; Fuller, G. G. Dynamic fluid-film interferometry as a predictor of bulk foam properties. *Soft Matter* **2016**, *12*, 9266−9279.

(10) Hartl, M. J. I. P. M. R.; Krupka, I.; Poliscuk, R.; Liska, M.; Molimard, J.; Querry, M.; Vergne, P. Thin-film colorimetric interferometry. *Tribol. Trans.* **2001**, *44*, 270−276.

(11) Desse, J. M.; Albe, F.; Tribillon, J. L. Real-time color holographic interferometry. *Appl. Opt.* **2002**, *41*, 5326−5333.

(12) Desse, J. M. Real-time colour holographic interferometry (from holographic plate to digital hologram). *Academic* **2011**, 3−18.

(13) Desse, J. M.; Picart, P.; Tankam, P. Digital three-color holographic interferometry for flow analysis. *Opt. Express* **2008**, *16*, 5471−5480.

(14) Demoli, N.; Vukicevic, D.; Torzynski, M. Dynamic digital holographic interferometry with three wavelengths. *Opt. Express* **2003**, *11*, 767−774.

(15) Desse, J. M. Three-color differential interferometry. *Appl. Opt.* **1997**, *36*, 7150−7156.

(16) Kitagawa, K. Thin-film thickness profile measurement by three-wavelength interference color analysis. *Appl. Opt.* **1997**, *52*, 1998−2007.

(17) Abdelsalam, D. G. A comparison of digital holographic microscopy and on-axis phase-shifting interferometry for surface profiling. *Measurement* **2013**, *46*, 4121−4126.

(18) Vannoni, M.; Sordini, A.; Gabrieli, R.; Melozzi, M.; Molesini, G. Measuring the thickness of soap bubbles with phase-shift interferometry. *Opt. Express* **2013**, *21*, 19657−19667.

(19) Kim, J.; Kim, K.; Pahk, H. J. Thickness measurement of a transparent thin-film using phase change in white-light phase-shift interferometry. *Curr. Opt. Photonics* **2017**, *1*, 505−513.

(20) Gao, F.; Muhamedsalih, H.; Jiang, X. Surface and thickness measurement of a transparent film using wavelength scanning interferometry. *Opt. Express* **2012**, *20*, 21450−21456.

(21) Kim, S. W.; Kim, G. H. Thickness-profile measurement of transparent thin-film layers by white-light scanning interferometry. *Appl. Opt.* **1999**, *38*, 5968−5973.

(22) Patsyk, A.; Sivan, U.; Segev, M.; Bandres, M. A. Observation of branched flow of light. *Nature* **2020**, *583*, 60−65.

(23) Zhang, Y.; Sharma, V. Nanoridge Formation and Dynamics of Stratification in Micellar Freestanding Films. *Langmuir* **2018**, *34*, 1208−1217.

(24) Zhang, Y.; Sharma, V. Thickness-Dependent Phase Transition Drives Nanoridge-to-Mesa Instability in Micellar Freestanding Films. *Langmuir* **2018**, *34*, 7922−7931.

(25) Zhang, Y.; Yilixiati, S.; Pearsall, C.; Sharma, V. Nanoscopic terraces, mesas, and ridges in freely standing thin-films sculpted by supramolecular oscillatory surface forces. *ACS Nano* **2016**, *10*, 4678−4683.

(26) Goodman, J. W.; Lawrence, R. W. Digital image formation from electronically detected holograms. *Appl. Phys. Lett.* **1967**, *11*, 77−79.

(27) Huang, T. S. Digital holography. *Proc. IEEE* **1971**, *59*, 1335−1346.

(28) Leith, E. N.; Upatnieks, J. Reconstructed wavefronts and communication theory. *J. Opt. Soc. Am.* **1962**, *52*, 1123−1130.

(29) Schnars, U.; Jüptner, W. Direct recording of holograms by a CCD target and numerical reconstruction. *Appl. Opt.* **1994**, *33*, 179−181.

(30) Mandracchia, B.; Wang, Z.; Ferraro, V.; Villone, M. M.; Di Maio, E.; Maffettone, P. L.; Ferraro, P. Quantitative imaging of the complexity in liquid bubbles' evolution reveals the dynamics of film retraction. *Light: Sci. Appl.* **2019**, *8*, 1−12.
(31) Wang, Z.; Mandracchia, B.; Ferraro, P.; Ferraro, V.; Di Maio, E.; Maffettone, P. L.; Chen, W.; Fried, E. In *Fast and Accurate Thickness Mapping of Liquid Bubbles and Thin Protein Films*, 2018 International Conference on Manipulation, Automation and Robotics at Small Scales (MARSS); IEEE, 2018; pp 1−5.
(32) Joye, J. L.; Hirasaki, G. J.; Miller, C. A. Dimple formation and behavior during axisymmetrical foam film drainage. *Langmuir* **1992**, *8*, 3083−3092.
(33) Anachkov, S. E.; Danov, K. D.; Basheva, E. S.; Kralchevsky, P. A.; Ananthapadmanabhan, K. P. Determination of the aggregation number and charge of ionic surfactant micelles from the stepwise thinning of foam films. *Adv. Colloid Interface Sci.* **2012**, *183*, 55−67.
(34) Glassner, A. Andrew Glassner' s Notebook Soap Bubbles: Part 2. *IEEE Comput. Graphics Appl.* **2000**, *2*, 99−109.
(35) Molimard, J.; Querry, M.; Vergne, P.; Krupka, I.; Hartl, M. Calculation of pressure distribution in EHD point contacts from experimentally determinated film thickness. *Tribol. Int.* **2005**, *38*, 391−401.
(36) Shen, L.; Denner, F.; Morgan, N.; van Wachem, B.; Dini, D. Transient structures in rupturing thin films: Marangoni-induced symmetry-breaking pattern formation in viscous fluids. *Sci. Adv.* **2020**, *6*, No. eabb0597.
(37) Nasti, G.; Coppola, S.; Vespini, V.; Grilli, S.; Vettoliere, A.; Granata, C.; Ferraro, P. Pyroelectric tweezers for handling liquid unit volumes. *Adv. Intell. Syst.* **2020**, No. 2000044.
(38) González-Cano, A.; Bernabéu, E. Automatic interference method for measuring transparent film thickness. *Appl. Opt.* **1993**, *32*, 2292−2294.
(39) Chan, D. Y.; Klaseboer, E.; Manica, R. Film drainage and coalescence between deformable drops and bubbles. *Soft Matter* **2011**, *7*, 2235−2264.
(40) Coons, J. E.; Halley, P. J.; McGlashan, S. A.; Tran-Cong, T. A review of drainage and spontaneous rupture in free standing thin-films with tangentially immobile interfaces. *Adv. Colloid Interface Sci.* **2003**, *105*, 3−62.
(41) Abdelsalam, D. G.; Yao, B. Interferometry and its applications in surface metrology. *Opt. Interferom.* **2017**, 81.
(42) Anton, N.; Bouriat, P. Different surface corrugations occurring during drainage of axisymmetric thin liquid films. *Langmuir* **2007**, *23*, 9213−9220.
(43) Karraker, K. A.; Radke, C. J. Disjoining pressures, zeta potentials and surface tensions of aqueous non-ionic surfactant/electrolyte solutions: theory and comparison to experiment. *Adv. Colloid Interface Sci.* **2002**, *96*, 231−264.
(44) Nierstrasz, V. A.; Frens, G. Marginal regeneration and the Marangoni effect. *J. Colloid Interface Sci.* **1999**, *215*, 28−35.
(45) Champougny, L.; Roché, M.; Drenckhan, W.; Rio, E. Life and death of not so "bare" bubbles. *Soft Matter* **2016**, *12*, 5276−5284.
(46) Debrégeas, G. D.; De Gennes, P. G.; Brochard-Wyart, F. The life and death of "bare" viscous bubbles. *Science* **1998**, *279*, 1704−1707.
(47) Ozan, S. C.; Jakobsen, H. A. On the effect of the approach velocity on the coalescence of fluid particles. *Int. J. Multiphase Flow* **2019**, *119*, 223−236.
(48) Singh, G.; Miller, C. A.; Hirasaki, G. J. On dimple formation in foam films. *J. Colloid Interface Sci.* **1997**, *187*, 334−337.
(49) Sheludko, A. Thin liquid films. *Adv. Colloid Interface Sci.* **1967**, *1*, 391−464.
(50) Israelachvili, J. N. *Intermolecular and Surface Forces*; Elsevier: Santa Barbara, CA, 2011.
(51) Majaron, H.; Ravnik, M. Structural Coloration. In *Seminar for the Department of Mathematics and Physics*; University of Ljubljana: Ljubljana, 2013.

https://dx.doi.org/10.1021/acs.jpcc.0c09555
J. Phys. Chem. C 2021, 125, 1075−1086